

An analytical electromagnetic model of “Sen” transformer with multi-winding coupling

Yuhang Pan, Song Han*, Jinling Feng, Xiao Hu

Department of Electrical Engineering, Guizhou University, Guiyang, Guizhou 550025, PR China



ARTICLE INFO

Keywords:

“Sen” transformer
Multi-winding coupling
Unified magnetic equivalent circuits
Analytical electromagnetic model
Series compensating voltage
Power flow control

ABSTRACT

In flexible AC transmission systems, the “Sen” transformer (ST) is an economical and effective method for voltage regulation and power flow control, which can achieve independent control of active and reactive power. The ST is a three-phase multi-winding transformer based on the on-load tap-changing technology. In order to reveal the internal characteristics of the ST, this paper proposes an analytical electromagnetic model considering the multi-winding coupling in the ST with the three-phase three-limb structure. Firstly, according to the electromagnetic coupling relationship in the ST, a magnetic equivalent circuit model consisting of self-inductance coefficients and mutual inductance is derived via the unified magnetic equivalent circuit (UMEC). Secondly, an electric circuit model for the internal voltage and current of the ST is established based on the electrical connection between the ST and the external system. Finally, an analytical electromagnetic model considering multi-winding coupling for the ST is obtained by combining the magnetic equivalent circuit model and the electric circuit model. Two case studies have been carried out on a three-phase three-limb model of the ST with the help of MATLAB. The effectiveness of the proposed model is verified by comparing the obtained analytic results with the existing results from time-domain simulation about the series compensating voltage of the ST. In addition, the voltages and currents of windings in the ST in the conditions of different transformer core structures and ferromagnetic materials are investigated for evaluating the influence of magnetic coupling on the results.

1. Introduction

With the large-scale integration of renewable energy sources, it has been becoming more and more difficult for the voltage regulation and the optimal power flow control in complex power networks with UHV (Ultra High Voltage) transmission lines as the backbones [1,2]. The unified power-flow controller (UPFC) is an important way to solve the problems of voltage regulation and power flow control [3,4]. However, the high installation and operation costs prevent the UPFC from widespread applications. The “Sen” transformer (ST), as proposed in [5], has the ability of controlling active and reactive power flow independently. Compared with UPFC, the ST is lower in cost, higher in reliability and efficiency [6–8], although reducing the accuracy and dynamic performance [9]. The ST is a typical electromagnetic unified power flow controller, and is usually based on a three-phase multi-winding transformer. By changing the position of secondary winding taps, the ST can generate different voltages, achieving the adjustment of power flow. The adjustment performances between the “Sen” transformer and phase angle regulator (PAR) were compared in [10,11]. The results showed that the overall reactive power of the ST was lower than

that of the PAR for enhancing the required amount of active power flow. Therefore, the “Sen” transformer is expected to be a device that will have widespread applications in flexible AC transmission systems (FACTS).

As a matter of fact, the ST is a technology based on transformers and tap-changers. From the perspective of the development of electrical topologies and structural variants, many researchers have optimized the topology of the ST for the purpose of improving its power flow control performance. For example, some novel topologies of the ST were proposed in [12–15] for the sake of achieving continuous power flow control of existing transmission lines and improving the utilization rate of existing transmission lines. These topologies include the hybrid electromagnetic unified power flow controller (HEUPFC), the improved hybrid unified power flow controller (IHUPFC) and the power transistor-assisted “Sen” transformer (TAST) which consists of a high-capacity ST and a small capacity UPFC. A new structure of the ST was presented in [16], which employs three neutral winding transformers for negative compensating voltage. From the perspective of the development of tap changer control algorithms, an optimal combination algorithm of tap-settings for the voltage compensating windings of the ST

* Corresponding author at: Department of Electrical Engineering, Guizhou University, Guiyang, China.
E-mail address: shan@gzu.edu.cn (S. Han).

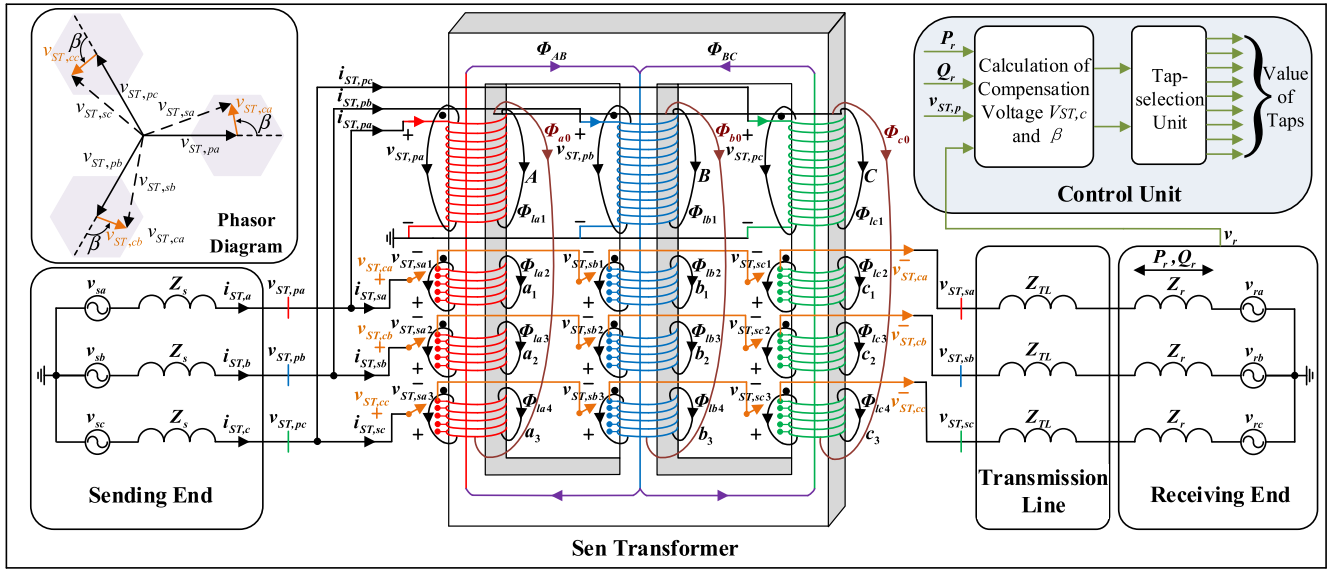


Fig. 1. Schematic of the ST and its connection to the transmission network [20].

was demonstrated in [17,18], which takes the voltage output of the secondary side of the ST in series as the control objective. Furthermore, a new control strategy with the reversal adjustment of tap changers for the ST is proposed in [19], which may increase the number of operating points for tap-changer and improve the control range and the accuracy of voltage regulation. From the perspective of the development of transient model for the ST, different types of modelling approaches have been proposed by scholars in order to further analyze the power flow control performance of the “Sen”

transformer. So there are various mathematical and simulation-based models to investigate the ST. In [21], a detailed real-time electromagnetic transient model of the ST was developed with C programming language in the MATLAB/SIMULINK environment. Furthermore, another electromagnetic transient model for the ST was provided in [20], which is based on the Norton equivalent circuit corresponding to the magnetic circuit of the ST. Besides, the real-time simulation of the ST was realized by field-programmable gate array (FPGA). Nevertheless, these modeling methods mainly study the external characteristics of the ST and there is no complete analysis for the internal characteristics of the ST. Thus the mechanism about the internal electromagnetic characteristics of the ST has not been revealed. In addition, not much is reported in the literature on the transformer model considering the coupling effect in the ST. Based on the ideal single-phase transformers in the PSCAD/EMTDC environment and MATLAB/Simulink, a few simplified models were developed for the ST in [22–25]. However, these simplified models do not involve the mutual coupling between compensating windings, and hence their accuracies are compromised. The ST may have a structure of three-phase three-limb multi-winding transformer, so it is necessary to consider the mutual coupling for modeling the ST. In this paper, a unified magnetic equivalent circuit (UMEC) based analytical electromagnetic model is proposed for the ST used in the transmission network. The proposed model involves the core topology of the ST and characterizes the asymmetric magnetic circuit of the three-phase three-limb transformer. The proposed model is expected to reflect the internal electromagnetic characteristics of the ST more accurately and improve the performance of the ST in case of series compensating voltage better. Two case studies have been carried out on a three-phase three-limb model of the ST using MATLAB. The effectiveness of the proposed analytical electromagnetic model is verified by comparing the obtained analytic results with the existing results from time-domain simulation about the series compensating voltage of the ST.

This paper is organized as follows. Section 2 describes the basic principle of the ST and proposes an analytical electromagnetic model for the ST including the magnetic part and the electrical part described in Sections 2B and C, respectively. Case 1 of Section 3 analyzes the influence of magnetic coupling on the analytical results. Moreover, the effects of different transformer core structure and different ferromagnetic materials on the voltage and current of the ST windings are investigated. Case 2 of Section 3 details the time-domain simulation of series compensating voltage. Results of series compensating voltage from the proposed model are compared with the results of simulation experiments in [17] and [20]. Conclusions are summarized in Section 4.

2. An analytical electromagnetic model of the “Sen” transformer

The electromagnetic behavior of the ST is determined by two types of constraints, i.e., external electric circuits and internal magnetic fields. The electric circuit equations reflecting the electrical characteristics mainly involving the external port and the magnetic circuit equations representing the magnetic features about the internal magnetic field distribution are interlinked or interacted according to the principle of electromagnetic induction. So the analytical equations considering multi-winding coupling for the ST should be established to solve the problem, which may reveal the working mechanism of the transformer more accurately and satisfy the needs of system-level analysis better [26,27].

2.1. Operating principle of the ST

The schematic of the ST applied to a transmission line is shown in Fig. 1. The ST injects a combined compensating voltage, $V_{ST,c}$, which is generated by the transformer’s secondary windings that are connected in series. The compensating voltage of variable magnitude and angles can change the magnitude and angle of the sending-end voltage, V_s , to the effective sending-end voltage, $V_{ST,s}$, enabling independent control of active and reactive power [21].

As seen from Fig. 1, the ST has two main units: an exciter unit and a compensating-voltage unit. The exciter unit consists of Y-connected shunt primary windings with phases A, B, and C and the compensating-voltage unit consists of nine secondary windings, three of which are placed on each limb of the core e.g., $a_1, a_2,$ and a_3 on the first limb, $b_1, b_2,$ and b_3 on the second limb, and $c_1, c_2,$ and c_3 on the third limb. The three-phase transmission line voltages denoted by $V_{ST,pa}, V_{ST,pb},$ and

$V_{ST,pc}$ at the sending-end are applied in shunt to the exciter unit. The induced voltages from three windings that are placed on three different limbs are added through series connection to produce the compensating voltage for injection in series with the transmission line, e.g., windings $a_1, b_1,$ and c_1 for injecting into phase-A, a_2, b_2 and c_2 for injecting into phase-B, and a_3, b_3 and c_3 for injecting into phase-C. The magnitude of the three 120° phase-shifted induced voltages are varied through active turns in the compensating windings. In this way, the composite voltage becomes variable in magnitude as well as in phase angle ($0\text{--}360^\circ$).

In addition, it is essential for the potential application of the ST to do optimal power flow studies with different objective functions, such as maximizing the available transfer capability (ATC) [7], minimizing congestion cost [8] and the active power loss [22]. The series compensating voltage $V_{ST,c}$ for the ST is usually used as a control variable, which can be acquired according to the corresponding optimal power flow algorithm. Subsequently, the number of winding turns can be obtained using the tap-setting algorithm [17].

2.2. Magnetic equivalent circuit model of the ST

The magnetic equivalent circuit representation of the three-phase three-limb ST is shown in Fig. 2 on the basis of unified magnetic equivalent circuit (UMEC). Each limb consists of three types of permeances [20,28].

- (1) Magnetomotive force (mmf) sources, $N_A i_{ST,pa}, N_B i_{ST,pb}$ and $N_C i_{ST,pc}$, generated by the current flow through the primary windings in phases A, B, and C, respectively; $N_{a1} i_{ST,sa}, N_{a2} i_{ST,sb}, N_{a3} i_{ST,sc}, N_{b1} i_{ST,sa}, N_{b2} i_{ST,sb}, N_{b3} i_{ST,sc}, N_{c1} i_{ST,sa}, N_{c2} i_{ST,sb}$ and $N_{c3} i_{ST,sc}$ are generated by the current flow through the secondary windings in phases A, B, and C, respectively;
- (2) Iron core permeances, $P_A, P_B,$ and P_C represent iron core permeances for primary windings in phases A, B, and C, respectively; $P_{a1}, P_{a2}, P_{a3}, P_{b1}, P_{b2}, P_{b3}, P_{c1}, P_{c2}$ and P_{c3} represent iron core permeances for secondary windings in phases A, B, and C, respectively; P_{ab} and P_{bc} represent yoke between phase-A and phase-B, and phase-B and phase-C, respectively;

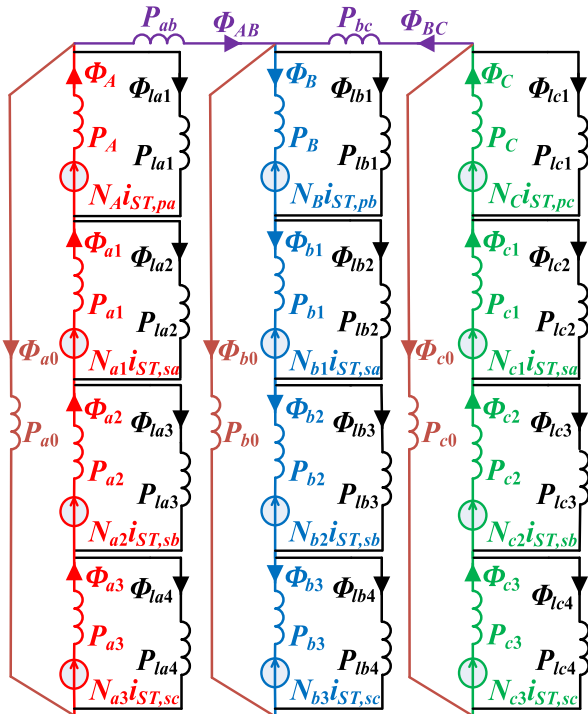


Fig. 2. Magnetic equivalent circuit representation for the iron core of the ST.

- (3) Leakage air permeances and zero-sequence permeances, $P_{la1}, P_{la2}, P_{la3}, P_{la4}, P_{lb1}, P_{lb2}, P_{lb3}, P_{lb4}, P_{lc1}, P_{lc2}, P_{lc3}$ and P_{lc4} represent the ST leakage air permeances in phases A, B and C, respectively; P_{a0}, P_{b0}, P_{c0} represent the ST zero-sequence permeances in phases A, B and C, respectively.

Assuming the limb length and leakage inductance are equally divided amongst the primary and secondary windings, the iron core permeances and the leakage permeances can be obtained as,

$$P_{Fe} = \mu_{Fe} \frac{S}{0.5L} \quad (1)$$

$$P_{leakage} = \frac{0.5X_{leakage}}{2\pi l N^2} \quad (2)$$

where μ_{Fe} is the core permeance determined by the B-H curve of the ferromagnetic material; S is the cross-sectional area and L is the limb length; N is the number of winding turns; $X_{leakage}$ is the leakage impedance.

The relationship between the magnetic flux, branch permeances and mmfs in the magnetic equivalent circuit of the ST satisfies the following equation [29],

$$\Phi = P(Ni - \theta) \quad (3)$$

where $\Phi, i,$ and θ represent the $n \times 1$ vector of the branch flux, winding currents, and branch mmfs, respectively. P and N represent the $n \times n$ diagonal matrix of branch permeances and the number of winding turns, respectively.

According to Gauss' law of magnetism, the flux at each node must sum to zero, i.e.,

$$A^T \Phi = 0 \quad (4)$$

where A^T is the node-branch connection matrix, and its entries can be 1, $-1,$ and 0 representing the branch flux entering, leaving, and disconnecting from the node, respectively.

The relationship between the branch mmfs θ and nodal mmfs θ_{node} is as follows,

$$A\theta_{node} = \theta \quad (5)$$

Combining Eqs. (3)–(5) can obtain Eq. (6)

$$\Phi = MPNi \quad (6)$$

where

$$M = I - PA(A^T PA)^{-1}A^T \quad (7)$$

and I is the identity matrix.

The excitation branch can be further divided into two parts: the branch that flows through the winding coil with the magnetic flux Φ^M , and the branch that does not flow through the winding coil with the magnetic flux Φ^P . In the circumstances, Eq. (6) can be rewritten as Eq. (8).

$$\begin{bmatrix} \Phi^M \\ \Phi^P \end{bmatrix} = \begin{bmatrix} M^{MM} & M^{MP} \\ M^{PM} & M^{PP} \end{bmatrix} \begin{bmatrix} P^M & 0 \\ 0 & P^P \end{bmatrix} \begin{bmatrix} N^M i^M \\ 0 \end{bmatrix} \quad (8)$$

For the UMEC model for the three-phase three-limb ST as depicted in Fig. 2, Eq. (9) can be obtained by applying Eq. (8).

$$\Phi^M = M^{MM} P^M N^M i^M \quad (9)$$

where M^{MM} is a 12×12 submatrix of M, Φ^M and i^M are 12×1 vectors, and P^M and N^M are diagonal 12×12 matrices, given as,

$$\Phi^M = [\Phi_A(t) \ \Phi_B(t) \ \Phi_C(t) \ \Phi_{a1}(t) \ \Phi_{b1}(t) \ \Phi_{c1}(t) \ \Phi_{a2}(t) \ \Phi_{b2}(t) \ \Phi_{c2}(t) \ \Phi_{a3}(t) \ \Phi_{b3}(t) \ \Phi_{c3}(t)]^T$$

$$i^M = [i_{ST,pa}(t) \ i_{ST,pb}(t) \ i_{ST,pc}(t) \ i_{ST,sa}(t) \ i_{ST,sa}(t) \ i_{ST,sa}(t) \ i_{ST,sb}(t) \ i_{ST,sb}(t) \ i_{ST,sb}(t) \ i_{ST,sc}(t) \ i_{ST,sc}(t) \ i_{ST,sc}(t)]^T$$

Table 1
Data for the electrical system and the ST.

Parameters	Value
Base value	138 kV
Sending-end line-to-line voltage	$1\angle 0^\circ$
Receiving-end line-to-line voltage	$1\angle -20^\circ$
Source impedance at the sending-end	1.0053 Ω and 19.17mH
Source impedance at the receiving-end	0 Ω and 0 mH
Transmission line impedance	3.0159 Ω and 59.19 mH
Resistance and inductance of the ST	1.7854 Ω and 47.4 mH
length of the limb	7.18 m
cross-sectional area of iron core	0.454 m ²
length of the yoke	2.66 m
cross-sectional area of iron yoke	0.454 m ²
Single-transformer leakage reactance of the ST	15.73 mH
Turns of primary winding of the ST	64
Turns of primary winding of the ST	26
Number of taps for ST	8
Adjustment step of tap for the ST	0.05 p.u./step
Maximum position of tap for the ST	0.4 p.u.
Adjustment time of tap for the ST	0.5 s/step
frequency	50 Hz

electrical system and the ST are shown in Table 1. Generally speaking, the relative permeability of silicon steel sheet ranges from 7000 to 10,000. The relative permeability of silicon steel sheet for the ST selected in this paper is $\mu_r = 10,000$ [30]. The case studies were conducted in the environment of MATLAB.

The electromagnetic analysis results of the ST are given in Table 2. It can be observed from a comparison of the analytical results between with and without considering the multi-winding coupling that the range of voltage amplitude difference is $-5.80\% \sim 3.44\%$, the range of voltage angle difference is $-7^\circ \sim 3.3^\circ$; the range of current amplitude difference is $-1.37\% \sim 1.63\%$, and the range of current angle difference is $-2.3^\circ \sim 2.4^\circ$. This implies that the multi-winding coupling effect has a little effect on the analytical calculation results, but it should not be ignored. However, when the phase-to-phase magnetic coupling is taken into account, the equivalent magnetic circuit lengths of the three-phase three-limb transformer are not equal due to the presence of the iron yoke. This causes asymmetrical mutual inductance between phases, which can lead to unbalanced winding voltages and branch currents. Therefore, the results of winding voltages and branch currents for the

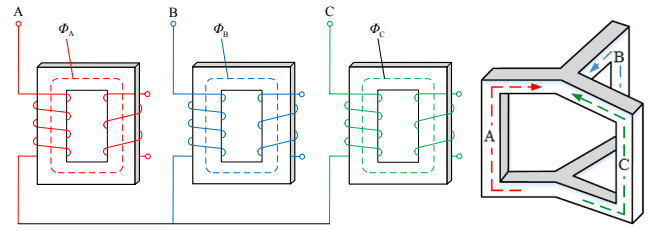


Fig. 5. A three-single-phase transformer bank and a three-phase three-limb transformer with the triangular core.

ST will be inaccurate if the coupling effect is ignored.

The influence of magnetic circuit on the winding voltages and currents was analyzed for the ST with the three-phase three-limb structure. The following analysis shows the effect of the phase-to-phase mutual inductance on the winding voltages and currents for the nine-single-phase transformer bank and the three-phase three-limb transformer with the triangular core. The core structure is displayed in Fig. 5.

If the ST uses the nine-single-phase transformer bank structure, the three-phase magnetic circuit is independent of each other and has no mutual inductance effect, and therefore there are not unbalanced three-phase voltages and currents. However, the shortcomings are larger consumption of materials, higher prices and larger space requirements. Furthermore, the analytical results for the ST using the nine-single-phase transformer structure are those without considering the winding coupling in Table 2. On the other hand, when the ST uses the three-phase three-limb transformer with the triangular core, the distances between the three branches of the core are equal and therefore the magnetic circuit lengths are the same, so the mutual inductance effects between the three phases are also the same. Consequently, there will be no unbalanced three-phase voltages and currents during the operation of the ST. The three-phase three-limb transformer with the triangular structure has the advantages of saving materials, lower prices and easier maintenance, but is more difficult to manufacture.

The biggest difference between the ST model of the nine-single-phase transformer bank and the one of the three-phase three-limb transformer with the triangular core is that the former has no magnetic field coupling, while the latter has magnetic field coupling and its topological magnetic field is symmetrical [31,32].

In order to study the influence of different iron core materials on the voltages and currents of the ST windings, different relative

Table 2
Comparison between the analytical results of the ST without and with multi-winding coupling.

Current (A) or Voltage (kV)	Without multi-winding coupling		With multi-winding coupling		Differences	
	Amplitude	Angle	Amplitude	Angle	Amplitude (%)	Angle
$I_{ST,pa}$	13.8	-90.7°	13.8	-90.7°	0	0°
$I_{ST,pb}$	13.8	149.3°	13.8	149.3°	0	0°
$I_{ST,pc}$	13.8	29.3°	13.8	29.3°	0	0°
$I_{ST,sa}$	226.7	-91.8°	226.3	-89.4°	-0.18	2.4°
$I_{ST,sb}$	226.7	148.2°	223.6	148.2°	-1.37	0°
$I_{ST,sc}$	226.7	28.2°	230.4	25.9°	1.63	-2.3°
$I_{ST,a}$	240.4	-91.7°	240.1	-89.5°	-0.12	2.2°
$I_{ST,b}$	240.4	148.3°	237.4	148.3°	-1.25	0°
$I_{ST,c}$	240.4	28.3°	244.2	26.1°	1.58	-2.2°
$V_{ST,pa}$	135.5	4.2°	132.9	5.0°	-1.92	0.8°
$V_{ST,pb}$	135.5	-115.8°	136.2	-119.7°	0.52	-3.9°
$V_{ST,pc}$	135.5	124.2°	137.6	125.4°	1.55	1.2°
$V_{ST,sa1}$	55.2	-2.2°	55.8	-1.5°	1.09	0.7°
$V_{ST,sb1}$	55.2	-122.2°	55.0	-120.4°	-0.36	1.8°
$V_{ST,sc1}$	55.2	117.8°	54.7	121.1°	-0.91	3.3°
$V_{ST,sa2}$	55.2	-2.2°	52.0	-5.2°	-5.80	-3.0°
$V_{ST,sb2}$	55.2	-122.2°	52.0	-124.7°	-5.80	-2.5°
$V_{ST,sc2}$	55.2	117.8°	52.1	115.8°	-5.62	-2.0°
$V_{ST,sa3}$	55.2	-2.2°	56.6	-9.2°	2.54	-7°
$V_{ST,sb3}$	55.2	-122.2°	56.5	-127.8°	2.36	-5.6°
$V_{ST,sc3}$	55.2	117.8°	57.1	113.5°	3.44	-4.3°

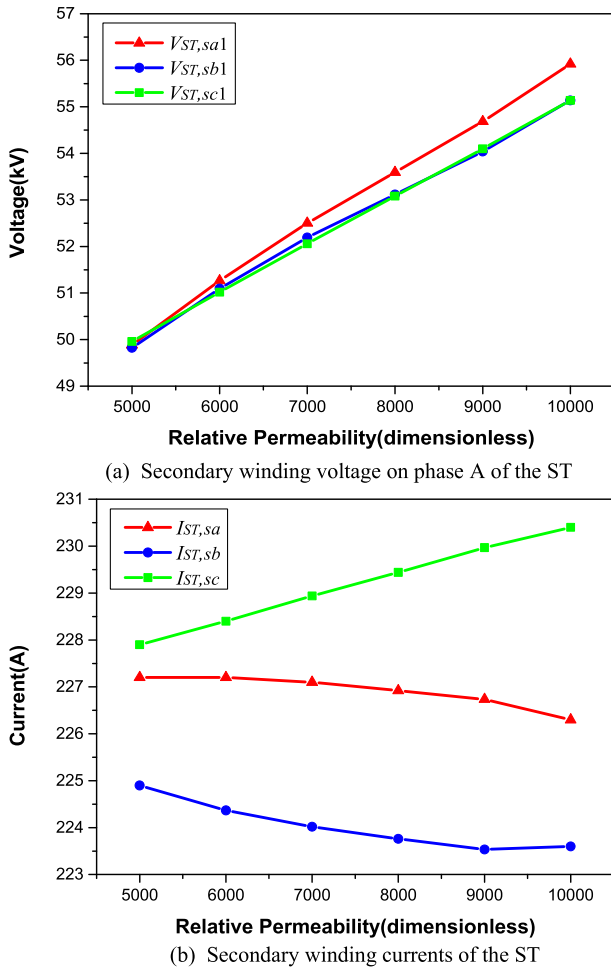


Fig. 6. Voltages and currents on the windings of the ST with different relative permeabilities.

permeabilities are used for this case, the obtained winding voltages and currents are plotted against the relative permeability in Fig. 6.

It can be found from Fig. 6 that the voltage of the ST winding goes higher as the relative permeability of the core material increases. At the same circumstance, the absolute amplitude of the voltage does not change significantly, while the secondary winding currents of the ST have different variations due to the amplitude and angle differences between the sending-end voltage and the receiving-end voltage.

It should be mentioned that the saturation and hysteresis characteristics of the iron core are not considered in order to simplify the calculations.

3.2. Case 2: Time-domain simulation of series compensating voltage

Based on the analytical results with the relative permeability of 10,000, the transient responses of the ST were studied considering various predetermined series voltage injections.

According to the adjustment scenario reported in [17], at the beginning of the time-domain simulation, the ST works in the uncompensated mode and the injected voltage is zero. At $t_1 = 5$ s a compensating voltage of 0.2 p.u. with an angle of 120° is requested by the controller, which means that the tap-setting on the secondary winding of TG_3 should start to increase to 0.2 p.u. with a step size of 0.05 p.u. and each step taking 0.5 s. Therefore, from $t_1 = 5$ s to $t_2 = 7$ s the tap-setting can increase to 0.2 p.u.. From $t_3 = 14$ s, the controller sends a request to ST to inject a compensating voltage of 0.2 p.u. with an angle of 60° . Therefore, the secondary winding tap-setting TG_1 needs

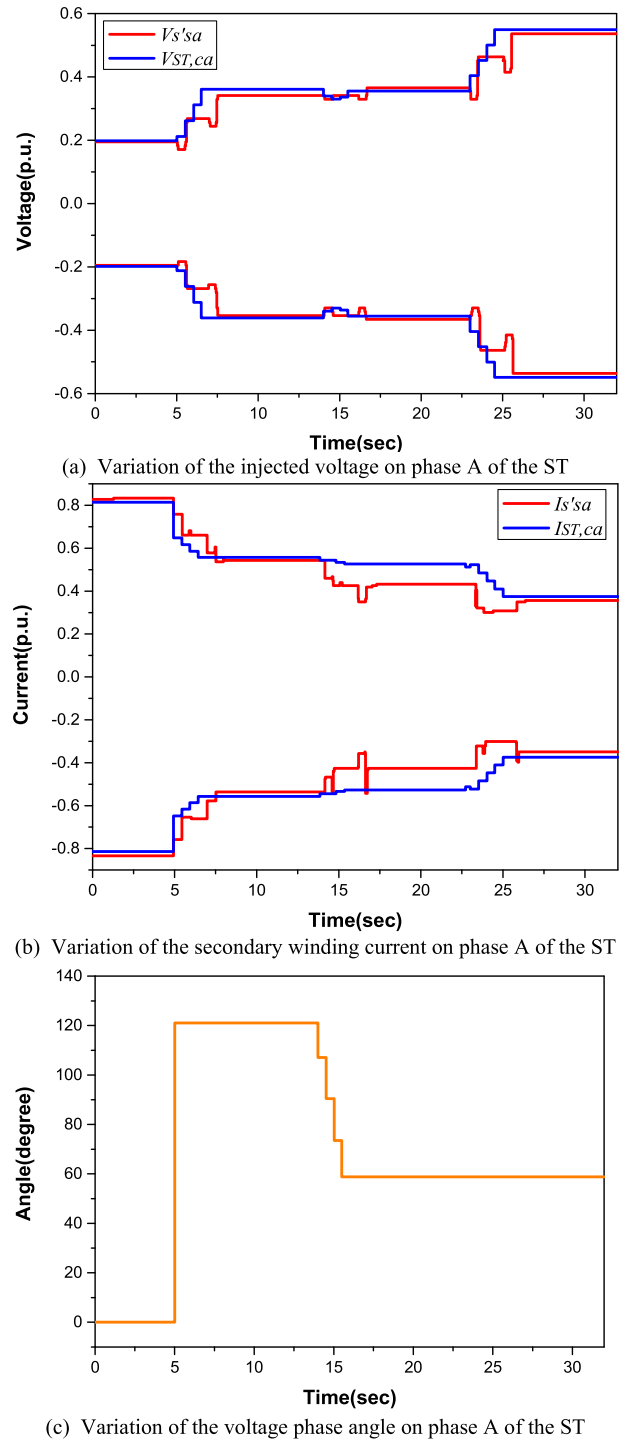
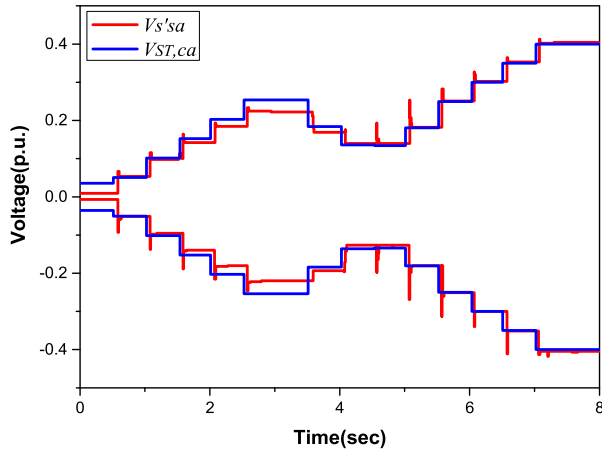
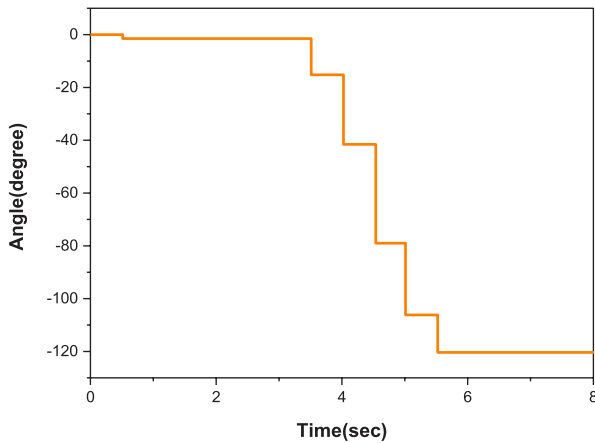


Fig. 7. Injected series voltages and secondary winding currents of the ST during the tap-changing process.

to be kept at 0.2 p.u. and TG_3 increases to 0.2 p.u.. From $t_3 = 14$ s to $t_4 = 16$ s, TG_3 increases to the 0.2 p.u. position. Finally, at $t_5 = 23$ s, the TG_1 and TG_3 winding voltages are further increased to 0.4 p.u. and the angle of the injected voltage is equal to 60° . The transition of the injected compensating voltage $V_{ST,ca}$ from $t = 0$ s to 32 s is shown in Fig. 7a. The transition of the ST secondary winding current $I_{ST,sa}$ is shown in Fig. 7b. Voltage compensation was performed according to the voltage regulation method in [20], i.e., when $t < 0.5$ s, $V_{ST,ca} = 0$, $\beta = 0^\circ$; when 0.5 s $< t < 3.5$ s, $V_{ST,ca} = 0.25$ p.u., $\beta = 0^\circ$; when 3.5 s $< t < 7.5$ s, $V_{ST,ca} = 0.4$ p.u., $\beta = 240^\circ$. The series compensating



(a) Variation of the injected voltage on phase A of the ST



(b) Variation of the voltage phase angle on phase A of the ST

Fig. 8. Injected series voltage during the tap-changing process.

voltage $V_{ST,ca}$ injected through the ST is shown in Fig. 8a. The series compensating voltage $V_{s'sa}$ and the secondary winding current $I_{s'sa}$ from [17] and [20] are also plotted in Figs. 7 and 8 for comparison.

It may be seen from Figs. 7 and 8 that the compensating voltage $V_{ST,ca}$ and the secondary current $I_{ST,sa}$ do reach the expected values, all of which closely agree with the corresponding results from Refs. [17,20]. This also suggests that the analytical electromagnetic model for the ST proposed in this paper is effective.

Appendix A

Magnetic equivalent circuit model of the ST

Algebraic equations of magnetic flux for each node

$$\begin{cases} \Phi_A - \Phi_{AB} - \Phi_{la1} - \Phi_{a0} = 0 \\ -\Phi_B + \Phi_{AB} + \Phi_{BC} - \Phi_{lb1} - \Phi_{b0} = 0 \\ \Phi_C - \Phi_{BC} - \Phi_{lc1} - \Phi_{c0} = 0 \\ -\Phi_A + \Phi_{a1} + \Phi_{la1} - \Phi_{la2} = 0 \\ \Phi_B - \Phi_{b1} + \Phi_{lb1} - \Phi_{lb2} = 0 \\ -\Phi_C + \Phi_{c1} + \Phi_{lc1} - \Phi_{lc2} = 0 \\ -\Phi_{a1} + \Phi_{a2} + \Phi_{la2} - \Phi_{la3} = 0 \\ \Phi_{b1} - \Phi_{b2} + \Phi_{lb2} - \Phi_{lb3} = 0 \\ -\Phi_{c1} + \Phi_{c2} + \Phi_{lc2} - \Phi_{lc3} = 0 \\ -\Phi_{a2} + \Phi_{a3} + \Phi_{la3} - \Phi_{la4} = 0 \\ \Phi_{b2} - \Phi_{b3} + \Phi_{lb3} - \Phi_{lb4} = 0 \\ -\Phi_{c2} + \Phi_{c3} + \Phi_{lc3} - \Phi_{lc4} = 0 \end{cases}$$

Connection matrix

4. Conclusions

This paper proposes an analytical electromagnetic model enabling consideration of the multi-winding magnetic coupling for the ST with the three-phase three-limb structure. Two case studies were carried out on a three-phase three-limb model of the ST using MATLAB. The effectiveness of the proposed model has been confirmed by comparing the obtained electromagnetic analysis results with published voltage regulation simulation results for the ST. The following conclusions have been drawn:

- The proposed model can take the core structure of the ST into account and characterize the asymmetry of the magnetic circuit in case of a three-phase three-limb transformer, which can reflect the internal electromagnetic characteristics of the ST more accurately.
- The multi-winding magnetic coupling has a relatively small effect on the results. While the most obvious changes are found in the amplitude and phase angle of individual winding voltage and branch current, the change in the amplitude does not exceed 6%, and the change in the angle does not exceed 7°.

CRediT authorship contribution statement

Yuhang Pan: Methodology, Formal analysis, Software, Data curation, Validation, Visualization, Writing - original draft. **Song Han:** Conceptualization, Supervision, Writing - original draft, Writing - review & editing, Project administration, Funding acquisition. **Jinling Feng:** Investigation, Writing - original draft, Validation. **Xiao Hu:** Writing - original draft, Writing - review & editing.

Declaration of Competing Interest

The authors declare that they have no known competing financial interests or personal relationships that could have appeared to influence the work reported in this paper.

Acknowledgements

This work was supported in part by National Nature Science Foundation under Grant (No. 51567006), the Program for Top Science & Technology Talents in Universities of Guizhou Province (2018036), and Guizhou Province Science and Technology Fund (20191100).

